Biomolecular NMR Assignments
https://doi.org/10.1007/s12104-023-10145-3

ARTICLE

Backbone and side chain NMR assignments and secondary structure calculation of the pheromone binding protein3 of *Ostrinia nubilalis*, an agricultural pest

Omar Al-Danoon[1] · Smita Mohanty[1]

Received: 24 April 2023 / Accepted: 12 July 2023

Abstract
Ostrinia nubilalis, also known as European Corn Borer (ECB), is a serious pest in Europe and North America, as well as in Central Asia and Northern Africa. It damages a variety of agricultural crops such as corn, oats, buckwheat, millet, and soybeans. causing annually at least one billion dollars in loss. The *Ostrinia nubilalis* pheromone-binding protein3 (OnubPBP3), preferentially expressed in the male moth antenna, has been implicated in the detection of the female-secreted pheromone blend during the mating process. Understanding the structure of and function of OnubPBP3, including the mechanism of pheromone binding and its release at the dendritic olfactory neuron (ORN), is essential if integrated pest management through sensory inhibition is to be achieved. We report here the backbone and side-chain resonance assignments of OnubPBP3 at pH 6.5 using various triple resonance NMR experiments on a ^{13}C, ^{15}N-labeled protein sample. The secondary structure of OnubPBP3 consists of six α-helices and an unstructured C-terminus based on backbone chemical shifts.

Keywords *Ostrinia nubilalis* · NMR assignment · Pheromone binding proteins (PBPs) · Agricultural pest

Biological context

The lepidopteran moth *Ostrinia nubilalis* in the family of Crambidae is an invasive pest. It is thought to have originated in Europe. It was first detected in the US in Massachusetts; it has now spread west to the Rocky Mountains in both the US and Canada and south to the Gulf coast. Managing this pest in an environmentally friendly and species-specific manner through sensory inhibition requires the understanding of proteins involved in the detection of pheromones. Pheromones are semiochemicals that evoke a behavioral response in males, guiding them to the females for mating. A complete understanding of the mechanism of pheromone binding and its release at the olfactory receptor neuron (ORN) is essential in the development of inhibitors.

The binding of pheromone with pheromone-binding proteins (PBPs) in the male moth antenna initiates a signaling cascade that results in behavioral response in insects. PBPs are highly soluble small acidic proteins with a molecular mass of 14–16 kDa. PBPs bind and transport the hydrophobic pheromones across the aqueous lymph to the odorant receptor. Lepidopteran PBPs such as *Bombyx mori* PBP (BmorPBP)(Damberger, Nikonova et al. 2000, Horst, Damberger et al. 2001, Lee, Damberger et al. 2002), *Antheraea polyphemus* pheromone-binding protein1 (ApolPBP1) (Mohanty, Zubkov et al. 2003, Mohanty, Zubkov et al. 2004, Zubkov, Gronenborn et al. 2005, Damberger, Ishida et al. 2007, Katre et al. 2009), *Amyelois transitella* PBP1 (AtraPBP1)(Xu et al. 2010, Xu, Xu et al. 2011, di Luccio, Ishida et al. 2013), and *Lymantria dispar* PBP2 (LdisPBP2) (Kowcun, Honson et al. 2001, Terrado et al., 2020) bind their respective pheromone at a relatively high pH (> 6.0) and release them at a lower pH (< 5.0). The pH of the sensillar lymph has been shown to be > 6.0 (Nardella et al., 2015), while the pH at the ORN is < 5.0 (Keil, 1984). In these PBPs, the pheromones occupy the hydrophobic binding pocket at higher pH in a bound (PBP^B) conformation

✉ Smita Mohanty
smita.mohanty@okstate.edu

[1] Department of Chemistry, Oklahoma State University, Stillwater, OK 74078, USA

Published online: 27 July 2023

while at acidic pH the nascent C-terminal helix inhabits the binding pocket in a well-defined free (PBP^A) conformation by displacing the pheromone at the site of the olfactory receptor neuron.

It has been reported that the pH-driven switch between the bound and the free conformations is regulated by two biological gates: a histidine gate consisting of His70 and His95 at one end of the binding pocket, and a C-terminal gate regulated by the C-terminus of the protein at the other end for several well-studied Lepidopteran PBPs including ApolPBP1 (Katre et al. 2009, 2013). When the histidine gate closes above pH 6.0, the C-terminal gate opens, allowing ligand binding (Katre, Mazumder et al. 2009); below pH 5.0, the C-terminal gate closes, releasing the ligand through the opened histidine gate at the opposite end of the pocket (Katre, Mazumder et al. 2013). Indeed, the unstructured C-terminus of ApolPBP1 is critical for ligand binding at high pH (Mazumder et al., 2019) and for ligand release at low pH when it switches to a helix and outcompetes the ligand for the pocket (Katre et al. 2013). Additionally, the histidine gate that opens at pH below 5.0 due to repulsion between the positively charged His70 and His95 allows the ligand to escape when the nascent C-terminal helix displaces it from the pocket (Katre, Mazumder et al. 2009, Katre, Mazumder et al. 2013). OnubPBP3 has over 50% sequence similarity with ApolPBP1, BmorPBP, AtraPBP1, and LdisPBP2, however, it has critical differences in both the biological gates as *Ostrinia furnacalis* PBP2 (OfurPBP2) (Mazumder, et al., 2018, Dahal et al., 2020, Al-Danoon et al. 2021, Dahal et al. 2022). Instead of a His70-His95 gate, OnubPBP3 has an Arg70-His95 gate and a more hydrophilic C-terminal tail containing five charged residues as opposed to three for ApolPBP1, BmorPBP, AtraPBP1, and LdisPBP2 (Al-Danoon et al. 2021). However, the OnubPBP3 C-terminus is less hydrophilic than OfurPBP2 C-terminus, which contains seven charged residues (Al-Danoon et al. 2021, Mazumder, et al., 2018, Dahal et al., 2020, Dahal et al. 2022). To understand how these critical substitutions in the histidine and C-terminal gates impact the structure and function for OnubPBP3, we have initiated a detailed structural characterization by solution NMR. Here, we report the backbone and side chain assignments of OnubPBP3 at pH 6.5.

Methods and experiments

Recombinant OnubPBP3 uniformly labeled with ^{15}N or $^{15}N/^{13}C$ was expressed in *E. coli* using minimal media containing $^{15}NH_4Cl$ (1.2 g/L) and either ^{12} or ^{13}C-glucose (4 g/L) and purified by anion exchange and size-exclusion chromatography as described previously (Al-Danoon, 2021). The purity of the proteins was confirmed by size exclusion chromatography and SDS-PAGE analysis (Al-Danoon, 2021). OnubPBP3 samples for NMR studies contained 0.46 mM uniformly ^{15}N- or $^{15}N/^{13}C$-labeled protein in 50 mM phosphate buffer at pH 6.5 containing 1 mM EDTA, 0.01% NaN_3, and 5% D_2O. All NMR experiments were conducted at 35 ^{0} C on a Bruker Avance III 800 MHz spectrometer fitted with a triple resonance H/C/N TCI cryoProbe equipped with z-axis pulsed field gradients at the National High Magnetic Field Laboratory (NHMFL) at Tallahassee, FL or a Bruker Neo 600 MHz spectrometer fitted with a TXI $^1H\{^{13}C/^{15}N\}$ 5 mm triple resonance indirect detection probe at the Oklahoma Statewide Shared Nuclear Magnetic Resonance Facility, Stillwater, Oklahoma.

The 2D $\{^{15}N$-$^1H\}$-HSQC spectrum (Fig. 1) was collected with 300 complex points in the ^{15}N dimension and 2048 complex points in the ^1H dimension. The following experiments were used for sequential assignment of ^1HN, $^1H_\alpha$, ^{15}N, $^{13}C_\alpha$, $^{13}C_\beta$, and ^{13}CO resonances: 2D $\{^{15}N,^1H\}$-HSQC, 2D $\{^{13}C,^1H\}$-HSQC, 3D HNCA, 3D HN(CO)CA, 3D HNCO, 3D HN(CA)CO, 3D HNCACB, 3D CACB(CO)NH, 3D CC(CO)NH, 3D H(CCCO)NH, 3D HCCH-TOCSY, 3D ^{15}N-edited HSQC TOCSY, 3D ^{15}N-edited NOESY and 3D $^{15}N/^{13}C$-edited NOESY (with mixing times of 120 ms). Data were processed with NMRPipe (Delaglio, Grzesiek et al. 1995) and analyzed with NMRFAM-SPARKY (Lee, Tonelli et al. 2015). The secondary structure, as shown in Fig. 2, was obtained by TALOS+ (Shen et al. 2009). Secondary chemical shifts, ΔC_α and ΔC_β and $(\Delta C_\alpha$-$\Delta C_\beta)$ as shown in Fig. 3, were calculated by subtracting random coil values from the C_α and C_β shifts (Wishart, Bigam et al. 1995).

Extent of assignments and data deposition

The resonances in the 2D $\{^{15}N$-$^1H\}$-HSQC spectrum of OnubPBP3 at pH 6.5 are well-dispersed (Fig. 1) indicating that the protein is properly folded. The assignment of backbone resonances (^1HN, ^{15}N, $^{13}C_\alpha$, $^{13}C_\beta$, and ^{13}CO) was completed for all residues in the 2D $\{^1H$, $^{15}N\}$-HSQC except for Ser1, Gln2, Leu132, and Leu137. The $^{13}C_\beta$ chemical shifts of the five cysteine residues (Cys19, Cys54, Cys97, Cys107, and Cys116) in the recombinant OnubPBP3 were higher than 39 ppm, while that of Cys50 was 34.7 ppm, suggesting that all of them are in the oxidized state (Sharma et al., 2000). The chemical shift assignments were deposited in the BioMagResBank (http://www.bmrb.wisc.edu) under accession number 51937. The secondary structure elements of the protein were predicated independently with two different programs using the chemical shifts: Secondary Structural information and TALOS+. The deviations of the Cα and Cβ chemical shifts (Δδ) from the mean random-coil values were calculated and the difference $\Delta\delta C\alpha - \Delta\delta C\beta$ was

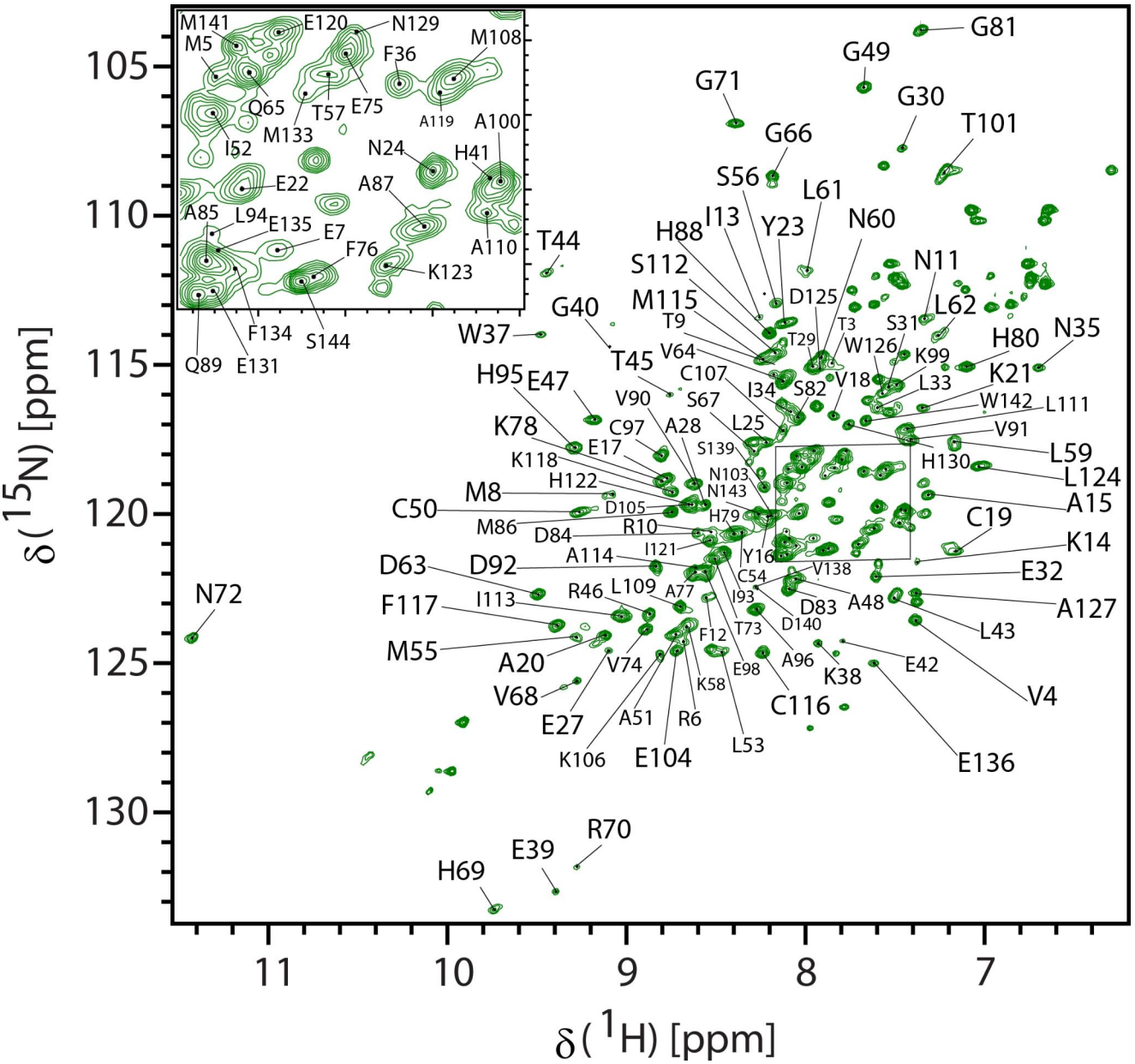

Fig. 1 2D [^{1}H, ^{15}N]-HSQC spectrum of uniformly ^{15}N,^{13}C-enriched OnubPBP3 in 50 mM phosphate buffer, 1 mM EDTA, 0.01% sodium azide at pH 6.5 and temperature 35 °C on a Bruker Avance 800 MHz spectrometer fitted with a cryo-probe. Backbone amide cross peaks of 144 residues OnubPBP3 were labeled with residues type and the sequence number. The residues S1, Q2, L132, and L137 were not found in the spectra. Resonances of the side-chain glutamine and asparagine amide groups have not been labeled. An expanded region of the HSQC spectrum is shown in the square inset

plotted against the OnubPBP3 sequence to obtain the secondary structural information in the protein (Fig. 3). This plot shows that OnubPBP3 contained seven α-helices starting with the N-terminus as the first helix. The C-terminus of the protein was predicted to be unstructured. The program TALOS + calculated the secondary structure by determining the φ and ψ torsion angles (Fig. 2).

Based on TALOS + calculations, the secondary structural elements in OnubPBP3 consist of six helices: 3–22, 27–34, 46–58, 71–79, 84–96, 108–124. The C-terminus of OnubPBP3 is unstructured, in stark contrast to the well-formed helix of the C-terminus of OfurPBP2. Despite over 50% sequence similarity between OnubPBP3 and OfurPBP2, including the N-terminal Arg70-His95 gate, the C-terminus of OnubPBP3 is unstructured in contrast to a helix for OfurPBP2 at pH 6.5. Both these proteins have relatively more hydrophilic C-termini, compared to those of ApolPBP1(Mohanty, Zubkov et al. 2004), BmorPBP (Lee,

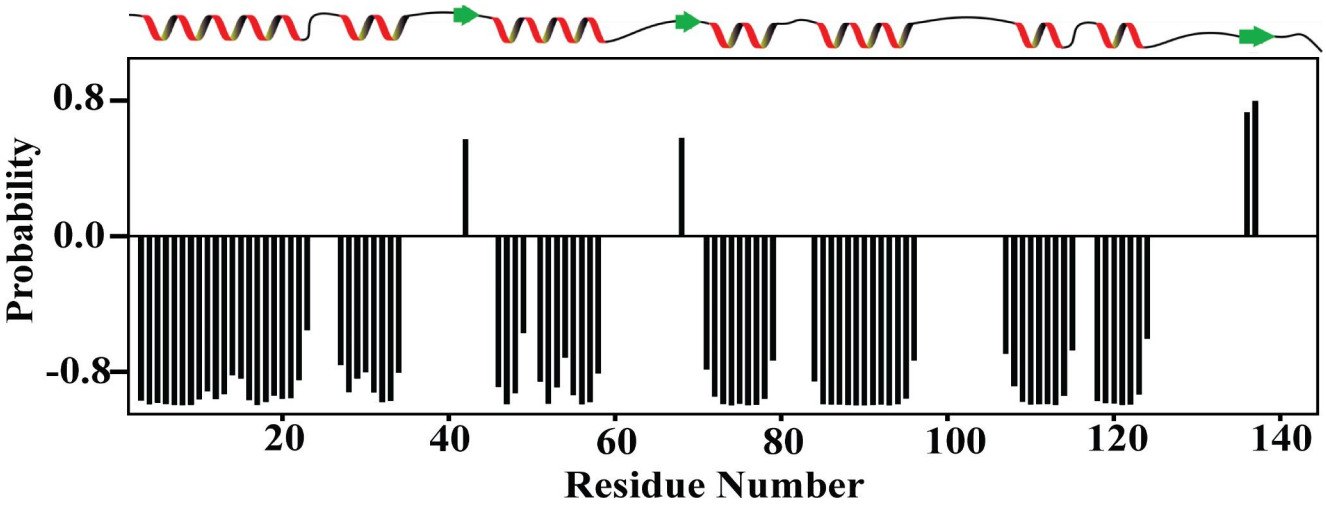

Fig. 2 Secondary structure prediction of OnubPBP3 obtained with TALOS+ (Shen et al. 2009) using the ^{1}H,^{15}N, $^{13}C_{\alpha}$, $^{13}C_{\beta}$, and $^{13}C'$ backbone chemical shifts. The secondary structure prediction is shown. The bars with positive or negative values correspond to β strands or α-helix, respectively. The height of the bars representing the probability of the secondary structure (-1 for α-helix, 0 for random coil, 1 for β-strand)

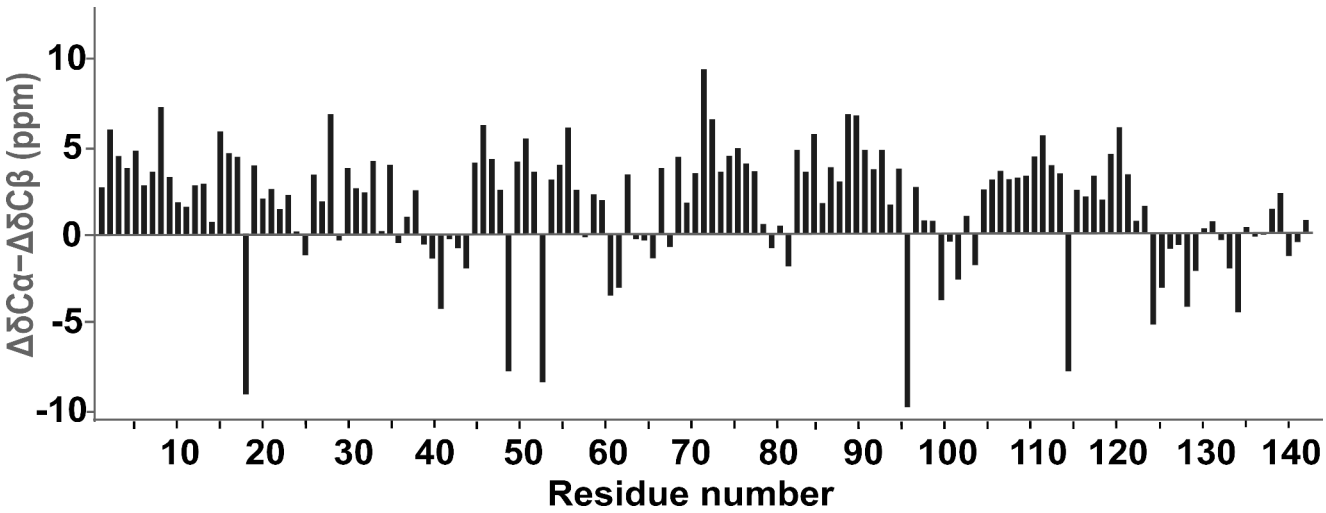

Fig. 3 Secondary chemical shifts, ΔCα-ΔCβ are plotted against the linear amino acid sequence. ΔδCα, and ΔδCβ are calculated by subtracting random coil values from the Cα and Cβ shift (Wishart et al. 1995)

Damberger et al. 2002), and AtraPBP1 (di Luccio, Ishida et al. 2013). However, OfurPBP2 has seven charged residues in its C-terminus, while OnubPBP3 has five (Al-Danoon et al. 2021, Mazumder, et al., 2018, Dahal et al., 2020, Dahal et al. 2022). Notably the difference in two charged residues likely renders the C-terminus of OnubPBP3 to a random coil that is exposed to the solvent in the ligand-bound conformation of the protein at pH > 6.0, similar to other well-studied PBPs that contain only 3 charged residues in their C-terminus such as ApolPBP1, BmorPBP and AtraPBP1. In ApolPBP1, BmorPBP, and AtraPBP1, the ligand is released at a lower pH (< 5.0) near the site of the olfactory receptor neuron through a pH-dependent conformational switch from the PBP^{B} conformation to the PBP^{A} conformation, in which the C-terminus becomes helical and occupies the binding pocket, displacing the ligand. However, the conformation of OnubPBP3 is adversely affected at pH 4.5 as we reported recently (Al-Danoon et al., 2021), unlike ApolPBP1, BmorPBP, and AtraPBP1 that have a well-defined pheromone-releasing conformation at pH 4.5 (Damberger, Ishida et al. 2007, Katre et al. 2009, 2013; Horst et al. 2001a, b, di Luccio, Ishida et al. 2013). Taken together, the above data indicate that OnubPBP3 may have a different mechanism of pheromone uptake and release.

Acknowledgements This research was financially supported by National Science Foundation Awards, CHE-1807722 and DBI-1726397 to Smita Mohanty. Majority of NMR data were collected at the National High Magnetic Field Laboratory, which is supported

by National Science Foundation Cooperative Agreement No. DMR-1644779 and the State of Florida. We thank Dr. Bharat Chaudhary for support with NMR data collection and helpful discussions. We thank Viswanath Nukala for deposition of the chemical shifts to BioMagResBank (www.bmrb.wisc.edu). We thank Dr. Shine Ayyappan for preparing Fig. 2. We thank Dr. Thomas Webb of Auburn University for the critical reading of this manuscript.

Author contributions SM conceived, designed the strategies and techniques employed, and supervised the research and analysis. OA processed and analyzed NMR data and completed the NMR resonance assignments. SM wrote the paper and OA prepared some of the figures.

Data Availability Both the backbone and side-chain chemical shift assignments have been deposited in the BioMagResBank (www.bmrb.wisc.edu) under accession number 51937.

Declarations

Conflict of interest The authors declare that they have no conflicts of interest with the contents of this article.

Ethics approval Not applicable.

Consent to participate Not applicable.

References

Al-Danoon O et al (2021) Structural and functional characterization of european corn Borer, Ostrinia nubilalis, Pheromone binding protein 3. J Agric Food Chem 69:14013–14023

Dahal S, Lewellen J, Ayyappan S, Chaudhary B, Mohanty S (2022) *Ostrinia furnacalis* PBP2 solution NMR structure: insight into ligand binding and release mechanisms. Protein Sci 31(10):e4438

Damberger F et al (2000) NMR characterization of a pH-dependent equilibrium between two folded solution conformations of the pheromone-binding protein from Bombyx mori. Protein science: a publication of the Protein Society 9(5):1038–1041

Damberger FF et al (2007) Structural basis of ligand binding and release in Insect Pheromone-binding proteins: NMR structure of Antheraea polyphemus PBP1 at pH 4.5. J Mol Biol 373(4):811–819

Delaglio F et al (1995) NMRPipe: a multidimensional spectral processing system based on UNIX pipes. J Biomol NMR 6(3):277–293

di Luccio E et al (2013) Crystallographic observation of pH-induced conformational changes in the Amyelois transitella pheromone-binding protein AtraPBP1. PLoS ONE 8(2):e53840–e53840

Horst R et al (2001a) NMR structure reveals intramolecular regulation mechanism for pheromone binding and release. Proc Natl Acad Sci USA 98(25):14374–14379

Horst R et al (2001b) Letter to the editor: NMR assignment of the A form of the pheromone-binding protein of Bombyx mori. J Biomol NMR 19(1):79–80

Katre UV et al (2009) Ligand binding turns moth pheromone-binding protein into a pH sensor: effect on the Antheraea polyphemus PBP1 conformation. J Biol Chem 284(46):32167–32177

Katre UV et al (2013) Structural insights into the ligand binding and releasing mechanism of Antheraea polyphemus pheromone-binding protein 1: role of the C-terminal tail. Biochemistry 52(6):1037–1044

Kowcun A et al (2001) Olfaction in the gypsy moth, Lymantria dispar: effect of pH, ionic strength, and reductants on pheromone transport by pheromone-binding proteins. J Biol Chem 276(48):44770–44776

Lee D et al (2002) NMR structure of the unliganded Bombyx mori pheromone-binding protein at physiological pH. " FEBS Letters 531(2):314–318

Lee W et al (2015) NMRFAM-SPARKY: enhanced software for biomolecular NMR spectroscopy. Bioinf (Oxford England) 31(8):1325–1327

Mazumder S et al (2018) Structure and function studies of asian corn Borer Ostrinia furnacalis pheromone binding Protein2. Sci Rep 8(1):17105

Mohanty S et al (2003) 1H, 13C and 15N backbone assignments of the pheromone binding protein from the silk moth Antheraea polyphemus (ApolPBP). J Biomol NMR 27(4):393–394

Mohanty S et al (2004) The solution NMR structure of Antheraea polyphemus PBP provides New Insight into Pheromone Recognition by Pheromone-binding proteins. J Mol Biol 337(2):443–451

Sharma D, Rajarathnam K (2000) ^{13}C NMR. chemical shifts can predict disulfide bond formation.“ J Biomol NMR, 18 (2): 165–171.

Shen Y et al (2009) TALOS+: a hybrid method for predicting protein backbone torsion angles from NMR chemical shifts. J Biomol NMR 44(4):213–223

Wishart DS et al (1995) 1H, 13 C and 15 N random coil NMR chemical shifts of the common amino acids. I. Investigations of nearest-neighbor effects. J Biomol NMR 5(1):67–81

Xu X et al (2010) NMR structure of navel orangeworm moth pheromone-binding protein (AtraPBP1): implications for pH-sensitive pheromone detection. Biochemistry 49(7):1469–1476

Xu W et al (2011) Extrusion of the C-terminal helix in navel orangeworm moth pheromone-binding protein (AtraPBP1) controls pheromone binding. Biochem Biophys Res Commun 404(1):335–338

Zubkov S et al (2005) Structural consequences of the pH-induced conformational switch in A.polyphemus pheromone-binding protein: mechanisms of ligand release. J Mol Biol 354(5):1081–1090